Nanostructured Scrolls from Graphene Oxide for Microjet Engines

ARTICLE *in* JOURNAL OF PHYSICAL CHEMISTRY LETTERS · AUGUST 2012

Impact Factor: 7.46 · DOI: 10.1021/jz300749p

6 AUTHORS, INCLUDING:

Bo Yang
University of Texas at Arlington
66 PUBLICATIONS **1,056** CITATIONS
SEE PROFILE

Tina T. Salguero
University of Georgia
17 PUBLICATIONS **361** CITATIONS
SEE PROFILE

THE JOURNAL OF PHYSICAL CHEMISTRY Letters

Letter

pubs.acs.org/JPCL

Nanostructured Scrolls from Graphene Oxide for Microjet Engines

Kun Yao,*[,†] Manoj Manjare,[†] Christopher A. Barrett,[§] Bo Yang,[⊥] Tina T. Salguero,[§] and Yiping Zhao[†]

[†]Nanoscale Science and Engineering Center, Department of Physics and Astronomy and [§]Department of Chemistry, The University of Georgia, Athens, Georgia 30602, United States

[⊥]Department of Mechanical and Aerospace Engineering, University of Texas, Arlington, Texas 76019, United States

Supporting Information

ABSTRACT: Layered heterostructures containing graphene oxide (GO) nanosheets and 20−35 nm bimetal coatings can detach easily from a Si substrate upon sonication—spontaneously forming freestanding, micrometer-sized scrolls with GO on the outside—due to a combination of material stresses and weak bonding between GO layers. Simple procedures can tune the scroll diameters by varying the thicknesses of the metal films, and these results are confirmed by both experiment and modeling. The selection of materials determines the stresses that control the rolling behavior, as well as the functionality of the structures. In the GO/Ti/Pt system, the Pt is located within the interior of the scrolls, which can become self-propelled microjet engines through O_2 bubbling when suspended in aqueous H_2O_2.

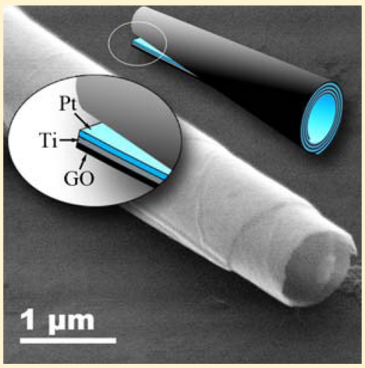

SECTION: Physical Processes in Nanomaterials and Nanostructures

Recent work on controlling the three-dimensional morphology of nano- and microsized objects has included an increasing number of studies on scrolls. The scroll form is attractive because it is a structure with open ends and edges, adjustable interlayer distances, and flexible interior volume that can be used for cargo transport. A variety of nanosheet materials can roll spontaneously into scroll structures; examples include graphene,[1,2] vanadium oxide,[3] potassium niobate,[4,5] titania,[6] lead oxide,[7] nickel,[8] and kaolinite.[9] In particular, carbon-based nanoscrolls, which are expected to have future applications as actuators, hydrogen storage materials, and drug-delivery platforms,[10−12] have been produced by methods ranging from chemical intercalation in graphite,[1,2] micro-explosion,[13] microwave spark assistance,[14] and surface strain engineering.[15]

In addition, several nanostructured heterolayer systems are known to exhibit scrolling behavior. Major efforts have involved metal and metal oxide (especially semiconductor) multilayers deposited on a sacrificial material layer.[16−18] Upon etching (removing the sacrificial layer), the released heterostructures spontaneously roll into micrometer-sized scrolls/tubes, which can be described evocatively as "jelly rolls".[19] For example, InAs/GaAs nanotubes and nanohelices,[20] $In_xGa_{1-x}As$/GaAs rectangular membranes and scrolls,[21,22] and multilayer Pt/Au/Fe/Ti microtubes[23] have been produced using this approach.

In this Letter, we describe multilayered heterostructures that contain graphene oxide (GO) nanosheets and exhibit spontaneous rolling behavior. The functions of the GO are to act as a support for the metallic multilayer and to provide an easily cleavable interface between the substrate and the vapor-deposited metal layers, which allows the heterostructures to detach from the surface and roll into freestanding scrolls. To our knowledge, this design strategy has not been applied to self-rolling nanostructured scrolls, despite the advantages, which include the fact that it extends the range of material components in such structures and it is experimentally convenient (because it eliminates the need for an etching step, uses an aqueous dispersion of GO, and does not require epitaxially grown or lithographically defined starting materials).

The proof-of-concept system consists of GO, titanium, and platinum (GO/Ti/Pt). To fabricate this multilayed structure, we first drop-cast an aqueous dispersion of GO nanosheets on a silicon wafer and then used electron-beam evaporation to coat the GO with titanium (10 nm) followed by platinum (10 nm). Scanning electron microscopy (SEM) images before and after coating (Figure 1a and b) show that there are no scrolled structures at these points, only wrinkles originating in the GO layer.

Upon sonication of the GO/Ti/Pt-coated wafer in water, the multilayer film fragments into multimicrometer-sized pieces that detach from the surface and spontaneously roll into full or partial scrolls (Figure 1b,c and Figure S1 in the Supporting Information). A size distribution analysis of more than 100 scrolls reveals that their diameters are typically 1−2 μm (average diameter: 1.4 ± 0.4 μm), and their lengths are 10−20 μm (average length: 15 ± 7 μm) (Figure S2 in the Supporting Information). Furthermore, we have tuned the diameters of the scrolls by varying the thickness of the platinum layer from 10 to

Received: June 9, 2012
Accepted: July 30, 2012

   dx.doi.org/10.1021/jz300749p | J. Phys. Chem. Lett. 2012, 3, 2204−2208

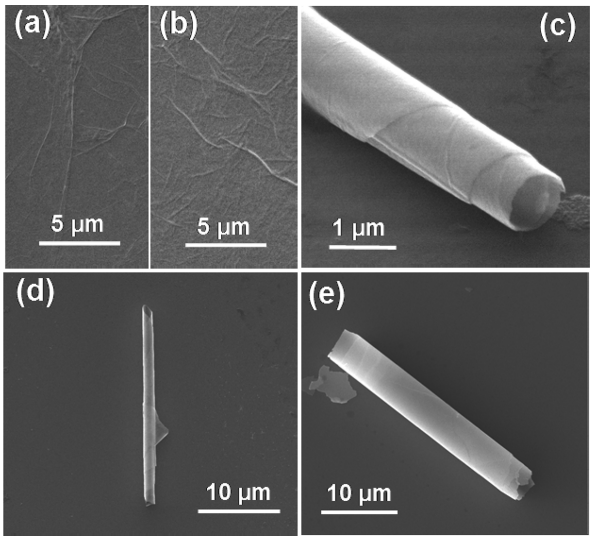

Figure 1. Representative SEM images: (a) GO on the Si substrate before Ti/Pt coating, (b) GO on the Si substrate after Ti/Pt coating. and (c) a typical GO/Ti/Pt scroll with 10 nm Ti and 10 nm Pt from a tilt view. Images (d) and (e) show typical GO/Ti/Pt scrolls with 10 nm Ti/10 nm Pt and 10 nm Ti/25 nm Pt.

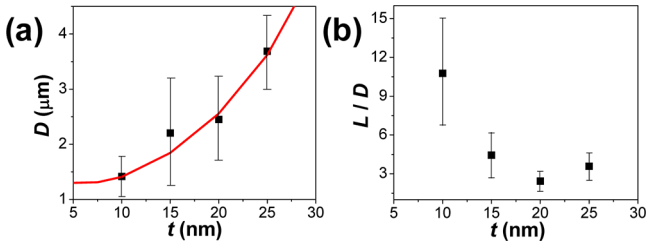

Figure 2. (a) Average scroll diameter D as a function of Pt thickness t and the best fit (red curve) using the stressed composite plate theory. (b) A plot of the scroll aspect ratio L/D versus the Pt thickness t.

25 nm (Figures S3 and S4 in the Supporting Information). For example, Figure 1e shows a SEM image of a typical scroll containing 10 nm Ti and 25 nm Pt. The average diameters of such scrolls are larger than those of scrolls with 10 nm Pt. In fact, the average scroll diameter (D) as a function of Pt thickness (t) plotted in Figure 2a shows a monotonic increase of D with t. No obvious dependence of average scroll length (L) on t was observed (Figure S5 in the Supporting Information). This is expected because the size distribution and shape of GO nanosheets in all experiments are statistically the same, and these parameters should determine the length of the scrolls.[24] Thus, the calculated scroll aspect ratio (L/D) versus t shows a decreasing trend (Figure 2b).

The heterostructured GO/Ti/Pt film can be modeled as a composite plate undergoing cylindrical bending, where the three layers of GO, Ti, and Pt are perfectly bonded together and the residual stresses are considered as the dominant driving force of the rolling. According to the Kirchhoff plate theory and the equilibrium condition of the nanosheet upon detachment from a substrate surface and rolling,[25] one has $\kappa = A\sigma_{Ti}^{*} + B\sigma_{Pt}^{*}$, where κ is the film curvature upon bending, equal to the inverse of roll radius, σ_{Ti}^{*} and σ_{Pt}^{*} are the residual stresses in the Ti and Pt layers, and A and B are the constants determined by the Young's modulus and thickness of each layer.[25,26] For our multilayer structures, the Ti thickness is fixed at 10 nm, and the Pt thickness varies from 10 to 25 nm. The Young's moduli (E) and Poisson ratios (ν) for Pt, Ti, and GO are given by E_{Pt} = 140 GPa and ν_{Pt} = 0.38; E_{Ti} = 90 GPa and ν_{Ti} = 0.32; and E_{GO} = 208 GPa, and ν_{GO} = 0.16.[27−29] The thickness of the GO layer and the residual stresses of Ti and Pt are the fitting parameters in the model. In order to fit the experimental data in Figure 2a, we find the best-fit curve shown in Figure 2a using a total GO thickness of 1.6 nm with σ_{Ti}^{*} = 3.6 GPa and σ_{Pt}^{*} = 6.9 GPa. Note that the residual stresses in the Ti and Pt layers are different by a factor of 2, but the corresponding residual strains are approximately the same, 0.027 and 0.030, respectively. Here, we assume that the residual stress in each layer is homogeneous. The calculated residual stresses are reasonable and comparable to previously reported values.[30] In addition, this model allows us to estimate the thickness of GO incorporated in the scrolls. The atomic force microscopy measurements show that the thickness of individual GO nanosheets is approximately 0.8 nm (Figures S7 and S8 in the Supporting Information); thus, the GO is incorporated into each scroll as a bilayer, on average.

Such GO bilayers in the scrolls relate to the interaction between GO and the metal coatings. In fact, our further characterizations using X-ray diffraction (XRD), X-ray photoelectron spectroscopy (XPS), and Raman spectroscopy all indicate that the nature of the GO changes after metal deposition. For example, Figure 3 shows the changing XRD

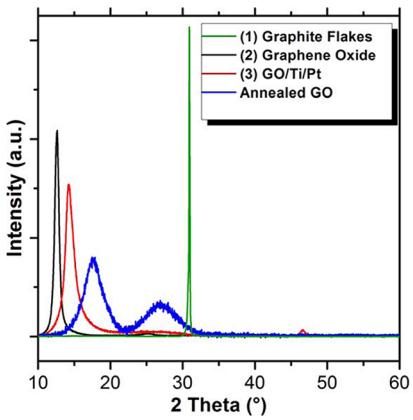

Figure 3. XRD data collected from graphite flakes (starting material for GO), exfoliated GO nanosheets on Si, GO/Ti/Pt layers on Si, and annealed (120 °C) GO nanosheets on Si.

patterns collected along the fabrication process, from (1) graphite starting material to (2) as-prepared GO nanosheets to (3) GO/Ti/Pt multilayers (not yet scrolled). The XRD pattern of the GO nanosheets exhibits a characteristic (002) peak at 12.5° (black curve), which can be correlated to an interlayer spacing of 0.807 nm. For comparison, the original graphite flakes exhibit a sharp peak at 31° (green curve), corresponding to an interlayer spacing of 0.335 nm. This change in basal plane d-spacing is typical for graphite versus GO.[31] However, after metal deposition, the (002) peak of GO clearly shifts to 15°, consistent with GO reduction. In this sample, the Pt (111) peak at 46° (red curve) also is visible. To corroborate GO reduction, GO nanosheets on Si were heated to 120 °C for 24 h. This annealing process resulted in a diffraction pattern typically exhibited by partially reduced GO, characterized by broad peaks shifted to higher angles of 2θ, 17.5°, and 26° (blue curve in Figure 3).[32] Additional data from XPS and Raman spectroscopy further support a GO reduction mechanism. To summarize, XPS shows a shift in relative intensity from C═O

dx.doi.org/10.1021/jz300749p | J. Phys. Chem. Lett. 2012, 3, 2204−2208

to C−C bonding after metal deposition (Figure S9 in the Supporting Information), consistent with the observation by Ajayan and co-workers,[33] and Raman spectroscopy indicates enhanced localized sp^3 defects, which is characteristic of reduction (Figure S10 in the Supporting Information). We conclude that metal deposition has a mild reducing effect on the GO nanosheets, causing the loss of predominantly carbonyl-containing functional groups and dissociation of water molecules.[32] Thus, the GO in GO/Ti/Pt appears to be intermediate in chemical and crystallographic character between as-prepared GO and fully reduced GO. Such a reduction effect should have two consequences; first, it suggests that the Ti layer interacts strongly with the adjacent GO layer, which leads to strong adhesion between the Ti and contacted GO monolayer; second, the reduction is a local effect confined to only the Ti−GO interface and immediately adjacent GO layers. Thus, the Ti acts as "glue" to attach approximately two GO monolayers and the Pt layer tightly within this layered structure.

In the GO/Ti/Pt structure, each material layer contributes to the overall scrolling behavior. The highly anisotropic dimensions of GO nanosheets (nm × μm × μm) cause them to assemble in parallel stacked arrangements within concentrated dispersions or dried forms.[34] The titanium layer enhances the adhesion between GO and Pt, and it induces GO reduction within approximately the first two contacted monolayers. These effects make the bilayer GO/Ti/Pt a tightly bonded three-component system. The residual stresses from the Ti and Pt layers cause this heterostructure to curl due to the relatively weak van der Waals interactions between GO nanosheet layers, which then allows the facile separation of the heterostructure from the substrate and further curling into scrolls. We emphasize that the detachment mechanism in this system is a physical delamination process, where the cleavage plane is within the top few nanometers of a much thicker GO film. Through this process, approximately two monolayers of partially reduced GO are incorporated on the outer surface of the scroll while excess GO remains on the substrate. The additional residual stress introduced by the Pt layer can tune the scroll diameter, and this material also can provide catalytic activity.

The stress model predicts that the Pt layer is wrapped inside of the scroll, and thus, such a structure can act as a "microjet engine" in the presence of H_2O_2, which reacts with the platinum catalyst to create O_2.[23,35,36] As visible in the video (Supporting Information), gas bubbles of O_2 generated by the reaction typically exit from one end of the scroll and drive it to move directionally in the liquid. Figure 4a shows representative movie frames extracted from the video (50× magnification objective lens). An analysis of the trajectory of this scroll in the horizontal plane reveals circular/spiral type motion (Figure 4b). By examining the total traveling distance S $[\equiv\sum_{i=2}^{n}((x_i - x_{i-1})^2 + (y_i - y_{i-1})^2)^{1/2}]$ versus time, as shown in Figure 4c, we further show that the scroll moves at a nearly constant speed (v) of 138 μm s^{-1}, which is approximately 12 body-lengths s^{-1}. This speed is comparable to flagellated bacteria, which are some of the fastest organisms on Earth.[37] In fact, even greater speeds (up to 200−350 body lengths s^{-1}) have been reported for scroll microjets in previous studies.[37,38]

We have examined the motions of tens of scrolls and found that all exhibit similar circular/spiral motion. However, speed and direction depend on many factors, such as the frequency and maximum size of the bubbles generated, the exact location

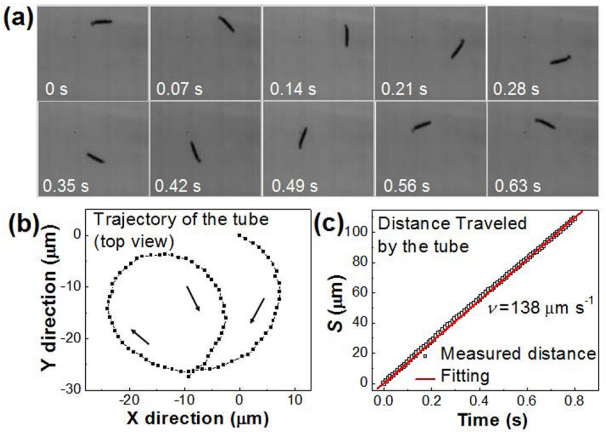

Figure 4. (a) A series of static frames extracted from the video of a GO/Ti/Pt scroll in motion in aqueous H_2O_2. (b) Top view of the trajectory of this scroll in the X−Y plane. (c) A plot of distance with respect to time calculated from (b) and the linear fit.

of the bubbles with respect to the central axis of the scroll, and whether the bubbles leave the scroll (eject) or burst without ejecting. Although the bubbles usually were ejected from one end of a scroll, we observed bubbles emerging from both ends in a few cases. It is likely that bubbles often appear at only one end because of the asymmetric geometry of most scrolls (see Figure 1 and Figure S11 in the Supporting Information); when the diameter of one end of the scroll is slightly larger than that at the other, the bubbles emerge from the end with the larger diameter. Other parameters, such as the shape of the scroll end and spontaneous fluctuation (symmetry broken due to noise), also could induce such a phenomenon. Nevertheless, bubbles were generated consistently from the ends, confirming that the platinum layer is located inside of the scrolls. We believe that both the circular/spiral motion and the differences in bubble production are caused by small inhomogeneities in the layers and variations in the nature of the scrolling.

In summary, we have demonstrated a facile method to fabricate multilayered, freestanding nanostructured scrolls, in which each material has been tailored to make both structural and functional contributions. In particular, the GO layer makes a maximum contribution with a minimal thickness that is consistent with miniaturization efforts. In addition, we have fabricated similar scrolls with Ti or Si layers on GO, which we will disclose in due course along with our continuing efforts to apply such materials to challenges in sensing, surface-enhanced Raman spectroscopy, and drug loading and delivery.

■ EXPERIMENTAL SECTION

Deposition of the Multilayered Heterostructure and Rolling-up. An aqueous dispersion of GO nanosheets was drop-cast onto clean 1 × 1 cm^2 silicon substrates. These substrates were placed on a hot plate and dried in air at approximately 100 °C for 10 min and then loaded into the evaporation system (Torr International, New Windsor, NY) for electron beam evaporation in a vacuum environment (10^{-6} Torr) at a vapor incidence angle of 0°. Both Ti and Pt were deposited at a rate of around 0.2 Å s^{-1}, read by a quartz crystal microbalance (QCM) facing directly toward the incident vapor. Next, the substrates coated with multilayer film were immersed in an 18 MΩ aqueous solution and fragmented into multimicrometer-sized pieces and spontaneously scrolled into scrolls during a sonication (less than 1 min).

dx.doi.org/10.1021/jz300749p | J. Phys. Chem. Lett. 2012, 3, 2204−2208

Jet Engine Activity. A volume of 5 μL of an aqueous dispersion containing the scrolls was pipetted onto a clean Si substrate, followed by the introduction of 5 μL of 10% H_2O_2 to activate the motion. After a steady reaction rate was reached and observed (approximately 1 min), pictures and videos of jet engine motion were captured by a Mitituya FS110 optical microscope with an Imperx charge-coupled device (CCD) camera (Phantom v9.1) mounted onto the trinocular head, using 10× and 50× magnification objective lenses.

■ ASSOCIATED CONTENT

Ⓢ Supporting Information

Additional experimental details and characterization results (SEM images, scroll size distributions, layer thickness measurements, XPS, Raman spectroscopy), as well as a video of jet engine behavior. This material is available free of charge via the Internet at http://pubs.acs.org.

■ AUTHOR INFORMATION

Corresponding Author

*E-mail: kunyao@uga.edu.

Notes

The authors declare no competing financial interest.

■ ACKNOWLEDGMENTS

This research was supported by the U.S. National Science Foundation under Contract #ECCS-0901141 (scroll preparation and microjet studies) and by startup funds to T.T.S. from the University of Georgia (materials characterization). We thank Albert Tamashausky (Asbury Carbons) for providing carbon samples, Asma Sharafi (UGA) for the initial preparation of graphene oxide samples, Prof. John Stickney (UGA) for access to XPS in his laboratory, and Prof. Marcus Lay (UGA) for access to Raman spectroscopy.

■ REFERENCES

(1) Viculis, L. M.; Mack, J. J.; Kaner, R. B. A Chemical Route to Carbon Nanoscrolls. *Science* **2003**, *299*, 1361−1361.

(2) Shioyama, T. A. H. A New Route to Carbon Nanotubes. *Carbon* **2003**, *41*, 179−198.

(3) Muhr, H.−J.; Krumeich, F.; Schönholzer, U. P.; Bieri, F.; Niederberger, M.; Gauckler, L. J.; Nesper, R. Vanadium Oxide Nanotubes — A New Flexible Vanadate Nanophase. *Adv. Mater.* **2000**, *12*, 231−234.

(4) Saupe, G. B.; Waraksa, C. C.; Kim, H.-N.; Han, Y. J.; Kaschak, D. M.; Skinner, D. M.; Mallouk, T. E. Nanoscale Tubules Formed by Exfoliation of Potassium Hexaniobate. *Chem. Mater.* **2000**, *12*, 1556−1562.

(5) Ma, R.; Sasaki, T. Conversion of Metal Oxide Nanosheets in Nanotubes. In *Inorganic and Metallic Nanotubular Materials*, Topics in Applied Physics; Kijima, T., Ed.; Springer-Verlag: Berlin, Heidelberg, Germany, 2010; Vol. *117*, Chapter 10, pp 135−146.

(6) Yao, B. D.; Chan, J. F.; Zhang, X. Y.; Zhang, W. F.; Yang, Z. Y.; Wang, N. Formation Mechanism of TiO_2 Nanotubes. *App. Phys. Lett.* **2003**, *82*, 281−283.

(7) Shi, L.; Xu, Y.; Li, Q. Controlled Growth of Lead Oxide Nanosheets, Scrolled Nanotubes, and Nanorods. *Cryst. Growth Des.* **2008**, *8*, 3521−3525.

(8) Zhang, G.; Sun, S.; Li, R.; Zhang, Y.; Cai, M.; Sun, X. Large-Scale Aqueous Synthesis and Growth Mechanism of Single-Crystalline Metal Nanoscrolls at Room Temperature: The Case of Nickel. *Chem. Mater.* **2010**, *22*, 4721−4727.

(9) Kuroda, Y.; Ito, K.; Itabashi, K.; Kuroda, K. One-Step Exfoliation of Kaolinites and Their Transformation into Nanoscrolls. *Langmuir* **2011**, *27*, 2028−2035.

(10) Braga, S. F.; Coluci, V. R.; Legoas, S. B.; Giro, R.; Galvão, D. S.; Baughman, R. H. Structure and Dynamics of Carbon Nanoscrolls. *Nano Lett.* **2004**, *4*, 881−884.

(11) Mpourmpakis, G.; Tylianakis, E.; Froudakis, G. E. Carbon Nanoscrolls: A Promising Material for Hydrogen Storage. *Nano Lett.* **2007**, *7*, 1893−1897.

(12) Shi, X.; Pugno, N. M.; Gao, H. Tunable Core Size of Carbon Nanoscrolls. *J. Comput. Theor. Nanosci.* **2010**, *7*, 517−521.

(13) Zeng, F.; Kuang, Y.; Wang, Y.; Huang, Z.; Fu, C.; Zhou, H. Facile Preparation of High-Quality Graphene Scrolls from Graphite Oxide by a Microexplosion Method. *Adv. Mater.* **2011**, *23*, 4929−4932.

(14) Zheng, J.; Liu, H.; Wu, B.; Guo, Y.; Wu, T.; Yu, G.; Liu, Y.; Zhu, D. Production of High-Quality Carbon Nanoscrolls with Microwave Spark Assistance in Liquid Nitrogen. *Adv. Mater.* **2011**, *23*, 2460−2463.

(15) Xie, X.; Ju, L.; Feng, X.; Sun, Y.; Zhou, R.; Liu, K.; Fan, S.; Li, Q.; Jiang, K. Controlled Fabrication of High-Quality Carbon Nanoscrolls from Monolayer Graphene. *Nano Lett.* **2009**, *9*, 2565−2570.

(16) Rogers, J. A.; Lagally, M. G.; Nuzzo, R. G. Synthesis, Assembly and Applications of Semiconductor Nanomembranes. *Nature* **2011**, *477*, 45−53.

(17) Huang, G.; Mei, Y. Thinning and Shaping Solid Films into Functional and Integrative Nanomembranes. *Adv. Mater.* **2012**, *24*, 2517−2546.

(18) Li, X. Strain Induced Semiconductor Nanotubes: from Formation Process to Device Applications. *J. Phys. D.: Appl. Phys.* **2008**, *41*, 193001.

(19) Lipomi, D. J.; Chiechi, R. C.; Reus, W. F.; Whitesides, G. M. Laterally Ordered Bulk Heterojunction of Conjugated Polymers: Nanoskiving a Jelly Roll. *Adv. Funct. Mater.* **2008**, *18*, 3469−3477.

(20) Prinz, V. Y.; Seleznev, V. A.; Gutakovsky, A. K.; Chehovskiy, A. V.; Preobrazhenskii, V. V.; Putyato, M. A.; Gavrilova, T. A. Free-Standing and Overgrown InGaAs/GaAs Nanotubes, Nanohelices and Their Arrays. *Physica E* **2000**, *6*, 828−831.

(21) Chun, I. S.; Challa, A.; Derickson, B.; Hsia, K. J.; Li, X. Geometry Effect on the Strain-Induced Self-Rolling of Semiconductor Membranes. *Nano Lett.* **2010**, *10*, 3927−3932.

(22) Schumacher, O.; Mendach, S.; Welsch, H.; Schramm, A.; Heyn, C.; Hansen, W. Lithographically Defined Metal−Semiconductor−Hybrid Nanoscrolls. *App. Phys. Lett.* **2005**, *86*, 143109.

(23) Solovev, A. A.; Mei, Y.; Bermúdez Ureña, E.; Huang, G.; Schmidt, O. G. Catalytic Microtubular Jet Engines Self-Propelled by Accumulated Gas Bubbles. *Small* **2009**, *5*, 1688−1692.

(24) Stoychev, G.; Zakharchenko, S.; Turcaud, S.; Dunlop, J. W. C.; Ionov, L. Shape-Programmed Folding of Stimuli-Responsive Polymer Bilayers. *ACS Nano* **2012**, *6*, 3925−3934.

(25) Timoshenko, S.; Woinowsky-Krieger, S. *Theory of Plates and Shells*; McGraw-Hill Book Company: New York, 1959.

(26) Beer, F. P.; Johnston, E. R.; DeWolf, J. T. *Mechanics of Materials*; McGraw-Hill Higher Education: New York, 2006.

(27) Suk, J. W.; Piner, R. D.; An, J.; Ruoff, R. S. Mechanical Properties of Monolayer Graphene Oxide. *ACS Nano* **2010**, *4*, 6557−6564.

(28) Tsuchiya, T.; Hirata, M.; Chiba, N. Young's Modulus, Fracture Strain, and Tensile Strength of Sputtered Titanium Thin Films. *Thin Solid Films* **2005**, *484*, 245−250.

(29) Salvadori, M.; Brown, I.; Vaz, A.; Melo, L.; Cattani, M. Measurement of the Elastic Modulus of Nanostructured Gold and Platinum Thin Films. *Phys. Rev. B* **2003**, *67*, 153404.

(30) Ivill, M.; Cole, M. W.; Hirsch, S. G.; Hubbard, C. Residual Stress of Pt Films with Ti and TiOx Adhesion Layers on Si and Sapphire Substrates. *Integr. Ferroelectr.* **2010**, *111*, 37−49.

(31) Dubin, S.; Gilje, S.; Wang, K.; Tung, V. C.; Cha, K.; Hall, A. S.; Farrar, J.; Varshneya, R.; Yang, Y.; Kaner, R. B. A One-Step, Solvothermal Reduction Method for Producing Reduced Graphene Oxide Dispersions in Organic Solvents. *ACS Nano* **2010**, *4*, 3845−3852.

(32) Huh, S. H. Thermal Reduction of Graphene Oxide. In *Physics and Applications of Graphene — Experiments*; Mikhailov, S., Ed.; InTech: Rijeka, Croatia, 2011; Chapter 5.
(33) Mathkar, A.; Tozier, D.; Cox, P.; Ong, P.; Galande, C.; Balakrishnan, K.; Reddy, A. L. M.; Ajayan, P. M. Controlled, Stepwise Reduction and Band Gap Manipulation of Graphene Oxide. *J. Phys. Chem. Lett.* **2012**, *3*, 986−991.
(34) Kim, J. E.; Han, T. H.; Lee, S. H.; Kim, J. Y.; Ahn, C. W.; Yun, J. M.; Kim, S. O. Graphene Oxide Liquid Crystals. *Angew. Chem., Int. Ed.* **2011**, *50*, 3043−3047.
(35) Gibbs, J. G.; Kothari, S.; Saintillan, D.; Zhao, Y. P. Geometrically Designing the Kinematic Behavior of Catalytic Nanomotors. *Nano Lett.* **2011**, *11*, 2543−2550.
(36) Fournier-Bidoz, S. B.; Arsenault, A. C.; Manners, I.; Ozin, G. A. Synthetic Self-Propelled Nanorotors. *Chem. Commun.* **2005**, *41*, 441−443.
(37) Sanchez, S.; Solovev, A. A.; Harazim, S. M.; Schmidt, O. G. Microbots Swimming in the Flowing Streams of Microfluidic Channels. *J. Am. Chem. Soc.* **2011**, *133*, 701−703.
(38) Gao, W.; Sattayasamitsathit, S.; Orozco, J.; Wang, J. Highly Efficient Catalytic Microengines: Template Electrosynthesis of Polyaniline/Platinum Microtubes. *J. Am. Chem. Soc.* **2011**, *133*, 11862−11864.